Available online at www.sciencedirect.com
SCIENCE DIRECT
Journal of Crystal Growth 286 (2006) 247–254
JOURNAL OF CRYSTAL GROWTH
www.elsevier.com/locate/jcrysgro

Highly reflective AlGaAsSb/InP Bragg reflector at 1.55 μm grown by MOVPE

O. Ostinelli[a,*], M. Haiml[b], R. Grange[b], G. Almuneau[c,**], M. Ebnöther[d], E. Gini[d], E. Müller[e], U. Keller[b], W. Bächtold[a]

[a]Department for Information Technology and Electrical Engineering, Swiss Federal Institute of Technology (ETH), Gloriastr. 35, 8092 Zürich, Switzerland
[b]Physics Department, Institute for Quantum Electronics, ETH Zürich, Switzerland
[c]LAAS-CNRS, 7 av. Colonel Roche, 31077 Toulouse, France
[d]FIRST Center for Micro- and Nanoscience, ETH Zürich, Switzerland
[e]Physics Department, Laboratory for Solid State Physics, ETH Zürich, Switzerland

Received 6 June 2005; received in revised form 13 September 2005; accepted 16 September 2005
Available online 28 November 2005
Communicated by R. Bhat

Abstract

The metalorganic vapor-phase epitaxy growth of a highly reflective 24-pair AlGaAsSb/InP-distributed Bragg reflector (DBR) is reported for the first time. The influence of the growth parameters such as the V/III input ratio, the growth temperature and the pressure, the total H_2 flow, the gas velocity and the switching sequence of the source gases at the interfaces has been deeply investigated and optimized to achieve stable growth conditions. The DBR achieves a reflectivity as high as 99.5% around 1.55 μm, a uniform stable composition, and an excellent crystal quality over the 2 inch wafer, with a surface free of crosshatch and a defect density below 1/cm^2. For the optical characterizations, measurements of linear and nonlinear reflectivity, transmission, pump-probe and photoluminescence were done. The interfaces and bulk layers of InP/AlGaAsSb/InP heterostructures were analyzed by transmission electron microscopy. High resolution X-ray diffraction measurements were used to determine the composition shift in the growth plane of the DBR. The measurements show the high quality of the growth and demonstrate that thick AlGaAsSb/InP heterostructures can be grown by metalorganic vapor-phase epitaxy (MOVPE), and in particular DBRs above 1.31 μm.
© 2005 Elsevier B.V. All rights reserved.

PACS: 71.55.Eq; 42.55.Px; 81.15.Gh; 85.60.−q

Keywords: A1. Crystal morphology; A1. Low-dimensional structures; A3. Metalorganic vapor-phase epitaxy; B1. Antimonides; B2. Semiconducting indium phosphide; B3. Heterojunction semiconductor devices

1. Introduction

The antimonide compounds lattice-matched to InP have been widely investigated in the last decades, and represent interesting low band gap, high refractive index materials for many optoelectronic and electronic devices like long wavelength vertical-cavity surface-emitting lasers (LW-VCSELs) at 1.31–1.55 μm [1], double heterojunction bipolar transistors (DHBTs) [2], semiconductor saturable absorber mirrors (SESAMs) [3] and tandem solar cells [4]. Due to the large refractive index contrast between AlGaAsSb and InP above 1.31 μm, this material combination is ideal for the fabrication of distributed Bragg mirrors (DBRs) based on InP. Even though GaAsSb grown by metalorganic vapor-phase epitaxy (MOVPE) is applied to e.g. DHBTs and solar cells, thick AlGaAsSb/InP heterostructures like DBRs with quality sufficient to achieve high reflectivities, have been grown only by molecular beam

*Corresponding author. Tel.: +41 44 498 14 23; fax: +41 44 498 14 12.
**Also to be corresponded to. Tel.: +33 5 61 33 64 73; fax: +33 5 61 33 62 08.
E-mail addresses: ostin@phys.ethz.ch, olivier.ostinelli@avap.ch (O. Ostinelli), almuneau@laas.fr (G. Almuneau).

0022-0248/$ - see front matter © 2005 Elsevier B.V. All rights reserved.
doi:10.1016/j.jcrysgro.2005.09.026

epitaxy (MBE) [5]. Owing to the lower costs, MOVPE is today extensively used in the III–V semiconductor industry for large volume production [6] giving the incentive for the fabrication of DBR structures or μm-thick AlGaAsSb/InP heterostructures for different applications. However, the growth of AlGaAsSb on InP is generally known to be challenging due to the presence of a large miscibility gap, the possible formation of ordering, the difficult control of the interfaces, resulting in the high defect densities, rough surfaces and a difficult reproducibility. Moreover, Sb segregates to the surface of both the wafer and the susceptor during the growth of AlGaAsSb causing an extraordinarily strong memory effect since Sb incorporates into the succeeding layer [7].

In this paper, we demonstrate the MOVPE growth of a highly reflective DBR composed of 24 AlGaAsSb/InP periods obtained through an accurate study of the impact of different parameters on growth. We will focus on the description and the understanding of the peculiar growth behaviors with the aim to achieve stable and reproducible growth conditions. Furthermore, the mechanism responsible for the creation of defects at the InP/AlGaAsSb interface has been identified, and a particular switching procedure leading to low defect density was developed. On the other hand, the AlGaAsSb/InP interface was optimized to minimize the memory effect. The results obtained from photoluminescence (PL), high resolution X-ray diffraction (HRXRD), transmission electron microscopy (TEM), accurate reflectivity and transmission measurements on the DBR and on a variety of heterostructures should emphasize the maturity of the antimonide growth process. The DBR grown under optimized conditions achieves a reflectivity of 99.5% with a surface free of any cross-hatch and a defect density below $1/cm^2$ over 90% of a 2 inch wafer. Along the growth plane, from the center to the edge, the As content increases by $\Delta y = 0.02$ in $Al_xGa_{1-x}As_ySb_{1-y}$ but no variation on the Al concentration was observed. Further, the demonstrated DBR is ideally suited for accurate transmission and reflectivity measurements to quantify and classify residual optical losses still present in AlGaAsSb.

2. Growth of (Al)GaAsSb/InP heterostructures

In this section, we describe the optimization of the growth parameters and their related effects. GaAsSb is lattice-matched to InP for an As content $y = 0.51$. At this composition, the PL peak emission at 300 K is centered at 0.78 eV (1.59 μm), meaning that band-to-band absorption occurs at least above this energy. The incorporation of Al into GaAsSb increases the band gap. An increase from $x = 0$ to 0.1 of Al in $Al_xGa_{1-x}As_ySb_{1-y}$ lattice-matched to InP shifts the band gap from 0.78 to 0.93 eV and reduces the refractive index contrast relative to InP by 17%. For the growth of highly reflective DBRs at 1.55 μm, the AlGaAsSb layers must be transparent in the stopband and at the same time the refractive index contrast with InP should be kept as high as possible. This can be achieved for an Al concentration of $x = 0.07$, which shifts the PL emission of the quaternary alloy to 1.4 μm (0.89 eV). A variation of $\Delta x = 0.01$ in the Al concentration leads to a negligible lattice mismatch of 40 ppm, but changes the band gap about 16 meV (30 nm around 1.55 μm). It is thus clear, that the Al content must be controlled with an accuracy of $\Delta x = 0.01$ over the entire growth. A fluctuation in the As concentration of $\Delta y = 0.01$ would lead to a lattice mismatch of 780 ppm. For the As concentration, an accuracy of $\Delta y = 0.02-0.03$ is required to prevent cross-hatch on the surface. These requirements impose severe conditions to the growth process over the entire DBR.

The epitaxial growth has been performed and optimized in a horizontal reactor heated with halogen lamps. About 2 inch InP (1 0 0) wafers with 2° miscut angle towards the direction [1 1 0] were used as substrates for all the growth runs. The substrate lay on a molybdenum disc rotating on a graphite susceptor. The sources used were trimethylindium (TMIn), trimethylgallium (TMGa), trimethylaluminum (TMAl) for the group III elements, and trimethylantimony (TMSb), arsine (AsH_3) and phosphine (PH_3) for the group V elements. We varied the growth temperature between 550 and 580 °C and the pressure between 100 and 160 mbar. The total H_2 flow for (Al)GaAsSb was set between 15 and 21.5 l/min, and to 12 l/min for InP. The V/III input ratio was set between 0.5 and 1 for the quaternary alloy.

2.1. Composition stability for GaAsSb

As shown by Watanabe et al. [8], the solid versus vapor composition for the GaAsSb material lattice matched to InP is highly nonlinear for growth temperatures around 600 °C and V/III input ratios above 1. On the contrary for lower temperatures and at a V/III input ratio of unity, this dependency becomes nearly linear over the entire composition range. At this growth regime the partial pressure of the group V species on the crystal surface is lower than 10^{-2} mbar and almost all atoms are incorporated. The As composition in incoming vapor $[AsH_3]/([AsH_3]+[TMSb])$, is close to the As composition in the solid $[As]/([As]+[Sb])$ [8]. The diffusion and reorganization of As and Sb atoms at the surface to build As- and Sb-rich islands can be prevented. Since the solid-state diffusion is very slow, it was shown that metastable GaAsSb can be grown [9,10].

In our experiments, the TEM diffraction pattern, the high-resolution and bright-field TEM images, did not show evidence of spinodal decomposition for both GaAsSb and AlGaAsSb alloys.

Another effect that influences the stability of the GaAsSb composition is the Sb segregation. During the growth of the ternary alloy a fraction of Sb is not incorporated into the bulk and segregates to the surface [7]. The quasi-liquid Sb film on the top of the GaAsSb thickens during the growth and changes the conditions for the adsorption and the incorporation of all the

constituents. It results in a layer with graded composition. At temperatures above 580 °C we observed a rapid increase of the segregation effect, which is probably caused by the increase of Sb desorption from the growing GaAsSb crystal and from the susceptor. As a consequence, we saw a non-reproducible increase of the As concentration of up to $\Delta y = 0.05$ in the growth direction within a GaAsSb layer thickness of 100 nm. It was therefore chosen to keep the temperature below 580 °C. In addition to that, the V/III input ratio was reduced to the minimum value (0.7) that still ensures the growth, to force the incorporation of all the group V atoms and thus the Sb impinging the surface. However, layers thicker than 0.3 μm require the introduction of a growth interruption after 0.2 μm to avoid composition drifts. During the pause, GaAsSb will be stabilized under AsH_3, which would reduce the amount of segregated Sb present on the surface (see Section 2.3).

Last but not the least, it was observed that the nonstoichiometric deposits (droplets or crystallites) formed from In, Ga, Al, Sb, As and P on the susceptor upstream with respect to the wafer plays a pivotal role for the composition stability. Especially at growth temperatures above 580–600 °C, some of the elements on the susceptor are carried in their gas phase by the H_2 flow to the wafer surface. This can rapidly damage the wafer surface, even before growth has started. Decreasing the reactor temperature, and thus the vapor pressures of the elements, can reduce this effect. Furthermore, we observed an increase of crystallites growth on the susceptor and on the wafer for V/III input ratios above unity. Turning to the opposite case, at an insufficient V/III input ratio (below 0.7), the elements of the group III coat the surface and droplets are formed. In both cases, the repercussion on the composition as well as on the growth rate is dramatic on the wafer. Once the correct V/III ratio was determined on the wafer, we improved its homogeneity on the full susceptor with the gas velocity to achieve suitable values for both susceptor and wafer. Indeed, the gas velocity, which is set by the reactor pressure and the total flow, controls the diffusion in cross-flow direction. We have found that droplets and crystallites could be avoided by keeping the growth temperature below 580 °C, by using a V/III ratio between 0.7 and 0.9, and a gas velocity ranging from 1 to 2.5 m/s.

2.2. *Incorporation of Al in GaAsSb*

As mentioned above, success in growing GaAsSb alloys relies predominantly on low growth temperatures and a V/III gas input ratio just below unity. The same behavior is applicable for the growth of AlGaAsSb, in particular for the Al concentration range between $x = 0$ and 0.3. A restrictive trend caused by the low growth temperatures is that the decomposition rate of the commonly used TMAl source is small below 600 °C, hence limiting the Al incorporation efficiency. However, this precursor presents the advantage of being stable over time and to have a methyl alkyl base such as our Ga, Sb and In sources, which may prevent from chemical reactions between these organic molecules. Even though raising the temperature would be a very efficient way to incorporate more Al in AlGaAsSb, it remains incompatible with the restrictions on our growth parameters.

The second obvious action would be to increase TMAl vs. the total group III flows. In first experiments, for a TMAl/TMGa ratio of 2, we achieved only $x = 0.05$ of Al in AlGaAsSb. Furthermore, three-dimensional growth prevailed and a dark semicircle appeared on the susceptor at the gas entry, most likely being the product of precipitate reactions. We also observed, for these high group III flows, a strong fluctuation of the Al concentration. This resulted in a broad PL emission presenting sometimes 2–3 contiguous maxima. The occurrence of these maxima could be explained by Al-induced band gap fluctuations, since it cannot be attributed to phase separation according to the TEM observations.

Beside the temperature and the TMAl input ratio, we will show in the next section that other growth parameters can induce an increase of the Al incorporation, without affecting the quality of the epilayers. We studied the influences of the total group V input flow and the gas velocity in the reactor, keeping TMAl and TMGa at 1.2×10^{-4} and 4.8×10^{-5} mol/min, respectively and the temperature at 565 °C. The gas velocity has been adjusted with the reactor pressure and the total H_2 flow. The composition of the AlGaAsSb layers was deduced by correlating HRXRD and PL measurements. For these experiments, all AlGaAsSb layers were lattice-matched i.e. with a constant As composition around $y = 0.52$.

In the first set of layers grown under constant gas velocity (1.8–1.9 m/s) the Al concentration increases from $x = 0.058$ to 0.067 when the group V flow is increased from 5×10^{-5} to 9×10^{-5} mol/min. In the second set we kept the group V constant at 9×10^{-5} mol/min, since this led to the highest Al concentrations. The Al concentration could be increased from $x = 0.06$ to 0.074 by decreasing the gas velocity from 2.6 to 1.39 m/s. At a gas velocity of 1.39 m/s and a group V source of 9×10^{-5} mol/min, we could achieve an Al incorporation of $x = 0.074$, corresponding to a blue-shift of the absorption edge of AlGaAsSb down to 1.4 μm.

The Al incorporation dependence on the gas velocity can be well understood in MOVPE, since the gas velocity controls the diffusion in cross-flow direction. On the other hand, the influence of the group V source flow is surprising. Pyrolysis studies made by Squire et al. [11] indicate that TMAl pyrolyzes heterogeneously. It is possible that a slight increment of the group V favors the decomposition process of TMAl increasing the adsorption and consequently the incorporation of Al into the bulk.

The group V sources, however, cannot be arbitrarily increased to obtain higher Al concentrations, since a minimized V/III input ratio is also required. For this reason, a compromise for the V/III input ratio must be achieved, leading to stable Al composition with good

incorporation efficiency. Considering these factors, by increasing the temperature to 570–575 °C and by taking the same TMAl and TMGa flows mentioned above, we were able to grow AlGaAsSb with an Al content up to $x = 0.14-0.15$. This corresponds to a band gap of 1 eV, which allows in principle the growth of DBRs for wavelength as low as 1.31 μm.

2.3. Heterostructures and interface

We have treated the principal mechanisms governing the growth of AlGaAsSb in the previous sections. By alternating AlGaAsSb and InP, however, additional aspects must be considered. Particularly challenging are the interfaces between InP and AlGaAsSb where all six constituents come into contact. Furthermore, since the two materials do not have common atoms, all the constituents of one material must be switched at the interface for growing the next material. The procedure of the gas switching sequences at the interfaces has been widely investigated and developed with the aim of making the growth of multiple heterostructures possible.

First experiments of AlGaAsSb grown on InP, revealed a defect density from 1000 to $8 \times 10^6/\mathrm{cm}^2$. The defect size increased with layer thickness. By decreasing the thickness of the quaternary alloy to some nanometers, it was possible to show that the defects are generated on the InP surface when AsH_3 is opened previous to TMSb, TMGa and TMAl. On the AlGaAsSb surface the defects appear as droplets and once the deposition of InP reconvenes, they evolved into an elongated shape (Fig. 1(a)). The creation of these defects represents a considerable drawback, especially for the growth of periodical heterostructures, since at each InP/AlGaAsSb interface new defects are added. Switching from PH_3 to TMSb for 5 s on an InP surface before adding AsH_3 and the group III source flow, leads to defect densities in the order of $10^6\,\mathrm{cm}^{-2}$. Fig. 1(a) shows an AlGaAsSb surface grown at 565 °C embedded between InP by using this switching sequence. The defect density is around $8 \times 10^6/\mathrm{cm}^2$ and the droplets are clearly visible in the center of each defect. We suggest that these droplets at the InP/AlGaAsSb interface are caused by the interaction of Sb with the InP surface giving probably an unstable quasi-liquid phase, which could be InSb.

To prevent the defects, a particular interface procedure has been developed. This switching sequence is depicted in Fig. 2(a). After the growth of the InP buffer layer, AsH_3 replaces PH_3 for 1 s at a partial pressure (P_{part}) of

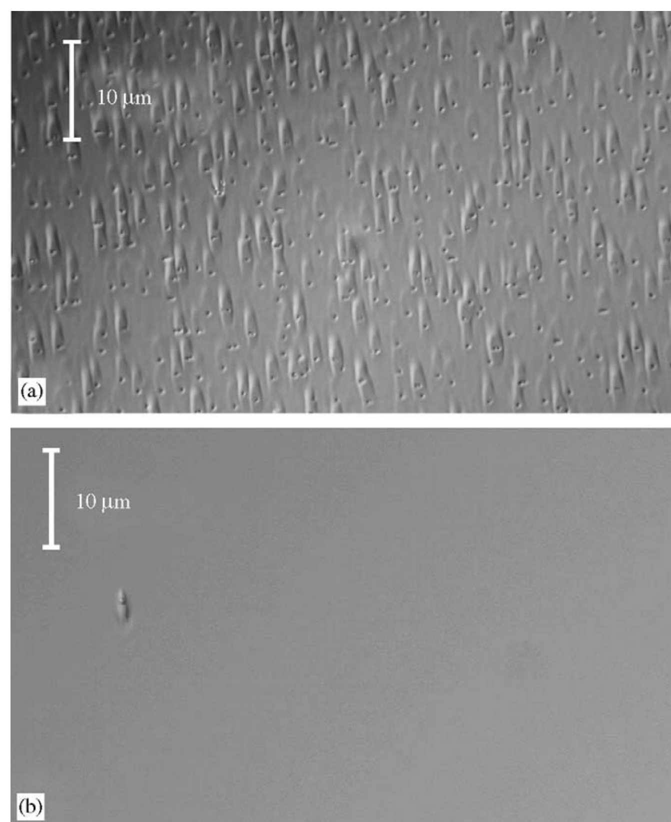

Fig. 1. Surface of the InP/AlGaAsSb/InP heterostructure. (a) TMSb has been introduced on InP at the InP/AlGaAsSb interface. (b) GaAs has been grown on InP to prevent the contact of Sb with InP at the InP/AlGaAsSb interface.

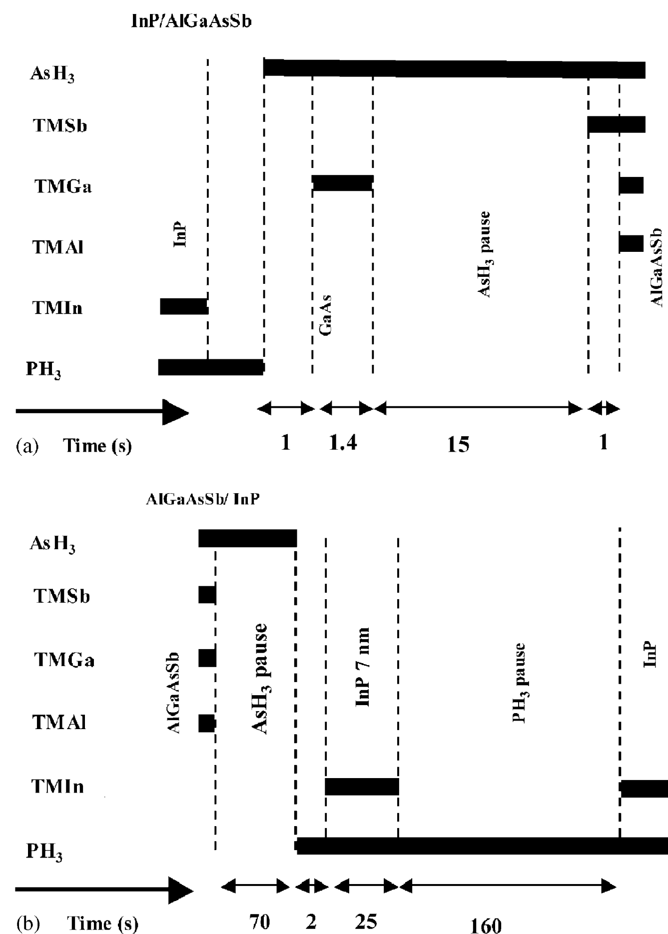

Fig. 2. Optimized switching procedure for the InP/AlGaAsSb and AlGaAsSb/InP interfaces. The thick black lines represent an open source.

9×10^{-1} mbar. After that, about four monolayers of GaAs grown during 1.4 s serving as a nucleation layer are grown on InP. This layer prevents any atomic contact between InP and Sb. After its growth the GaAs is stabilized 15 s under AsH_3 at a P_{part} about 160 times lower compared to that used for the GaAs growth. This much lower flow will be used for AlGaAsSb. This time is just long enough to guarantee the stabilization of the new AsH_3 concentration in the reactor. Longer purge times would result in a degradation of the GaAs surface. After this 15 s pause, TMSb is opened and flows in parallel to AsH_3 during 1 s. The As impoverished GaAs surface which will favor the incorporation of Sb and build GaAsSb. Longer pauses will produce an Sb layer even before the quaternary material has begun to grow. At this point the group III source flows are added to start AlGaAsSb. With this sequence, the defect density could be reduced to 0–1/cm^2. Fig. 1(b) shows the surface quality improvement of an AlGaAsSb capped with InP grown with this switching procedure.

The secondary ion mass spectrometry (SIMS) revealed the presence of Sb in InP when switching directly from AlGaAsSb to InP. When the growth of InP reconvenes, the segregated Sb presenting as a floating layer on the wafer surface will be incorporated. In addition to that, in a horizontal reactor the Sb deposited upstream with respect to the wafer desorbs and contributes to the contamination of InP. Although the growth of the quaternary alloy was performed below 580 °C and at minimized V/III input ratio the memory effect could not be completely suppressed. Indeed, in first experiments the HRXRD showed a fully relaxed $InP_{1-y}Sb_y$ with $y = 0.1$ over 60 nm, causing a lattice mismatch of 9.48×10^3 ppm. Purging the reactor with AsH_3 at interrupted AlGaAsSb growth decreases the amount of Sb on the wafer surface as reported in Ref. [12] for GaAsSb/InP MQWs. In Ref. [12] the HRXRD simulation assumed an 8 nm-graded $InP_{1-y}Sb_y$ layer before achieving pure InP with $y = 0.08$ and 0.04 on the GaAsSb side for 10 and 120 s AsH_3 purge time, respectively. A similar behavior was reported in Ref. [7] for the MBE growth where a GaAsSb surface was exposed to an incident As_2 beam. However, we saw that after 100 nm of AlGaAsSb even purge times exceeding 180 s are not sufficient to remove the residual Sb from the reactor and unfortunately the wafer surface begins to roughen.

To minimize the memory effect the switching sequence depicted in Fig. 2(b) was developed. To prevent the progressive roughening of AlGaAsSb, the reactor is purged with AsH_3 for 70 s at the same P_{part} used for the growth. Increasing the AsH_3 flow by 160 times (P_{part} of 9×10^{-1} mbar) to accelerate this process, would damage the AlGaAsSb surface in a couple of seconds. Further, during this time the total flow is gradually decreased from 15–21.5 l/min (depending on the process) to 9 l/min. After the purge pause, AsH_3 is exchanged to PH_3 during 2 s, before starting 7 nm of InP (25 s) to protect the AlGaAsSb. At 9 l/min, the depletion profile of the growth rate moves towards the area upstream with respect to the wafer, coating the susceptor and incorporating the Sb. After this 7 nm InP, TMIn is stopped and the reactor is purged with PH_3 for 160 s at the same P_{part} used for the InP growth, desorbing the Sb from InPSb. The total flow is set to 12 l/min, which is our standard flow for the InP growth. After this pause the InP growth reconvenes. With this sequence, the contamination of InP with Sb was reduced significantly. From the simulation of HRXRD rocking curves of 100 nm AlGaAsSb, we deduced a maximum grading of the Sb concentration from $y = 0.05$ to 0 over a 10–15 nm $InP_{1-y}Sb_y$ layer.

Adopting the described procedures at the interfaces, heterostructures as shown in the TEM in Fig. 3 were

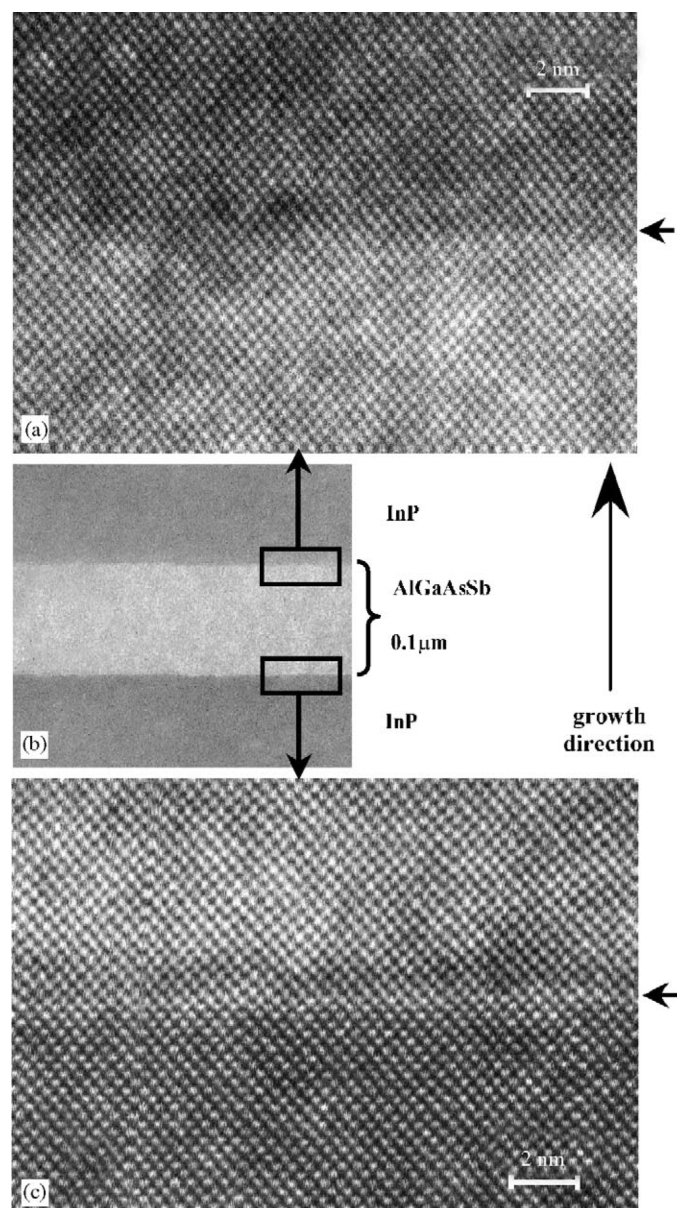

Fig. 3. TEM of the InP/AlGaAsSb/InP heterostructure with an electron beam parallel to [1 1 0]. (a) *Z*-contrast image of the AlGaAsSb/InP interface, (b) TEM image of AlGaAsSb bulk embedded between InP and (c) *Z*-contrast image of InP/AlGaAsSb interface.

grown. Fig. 3(a) and (c) show the Z-contrast images of the upper and lower interface between the quaternary and the binary alloy. In this almost fully incoherent scanning technique, the contrast nearly depends on the Z-value of the respective atomic species as $\sim Z^2$. Therefore a material containing heavier atoms shows a bright contrast. On the contrary lighter atoms appear to be darker. An increment in the layer thickness also increases the brightness. The darker areas therefore correspond to InP, the brighter to $Al_{0.06}Ga_{0.94}As_{0.55}Sb_{0.45}$ and slight contrast fluctuations within a layer are mainly due to thickness variations from the sample preparation. The crystalline lattice is clearly recognizable for both AlGaAsSb and InP. At the transition from InP to AlGaAsSb (Fig. 3(c)) we first observe a bright layer, which extends over 1–1.5 unit cells (0.6–0.8 nm) proving the presence of heavier atoms. We attribute this thin layer to InAs formed by substituting P atoms with As atoms by switching from PH_3 to AsH_3 after the growth of InP. The following layer of 1.5–2 unit cells is darker, and is attributed to the four monolayers of GaAs, grown to prevent defect formation. After these two strips of different contrast extending over 1.5–2 nm the AlGaAsSb layer begins with homogeneous composition.

At the AlGaAsSb/InP interface (Fig. 3(a)) no strip is visible in the Z-contrast, which would be attributed to an InPSb layer otherwise. However, the interface is not perfectly flat, which can be caused by the long AsH_3 purge time in the absence of TMSb after the growth of AlGaAsSb.

The steps done in the switching sequence at both interfaces are visible in the TEM.

2.4. DBR growth

According to the discussion above, a narrow window for the growth parameters has been found by minimizing all the negative effects observed during the growth. An example of such growth parameters is shown in Table 1. For multiple AlGaAsSb/InP layers we achieved compositional stability, a satisfactory efficiency for the Al incorporation, a low defect density and an estimated contamination of $y_{Sb} = 0.05$ in InPSb decreasing to zero over a thickness of 10–15 nm. The conditions shown in Table 1 were finally used for growing a DBR designed for LW-VCSELs at 1.55 μm. Since at this wavelength the refractive index difference between InP (low index) and AlGaAsSb (high index) lattice-matched to InP with $x_{Al} = 0.07$ is 0.4, reflectivities of 99% with not more than 20 AlGaAsSb/InP Bragg pairs can be achieved. Since VCSELs usually need Bragg mirrors with reflectivities above 99%, the DBR was grown with 24 Bragg periods. In order to obtain a stopband around 1.55 μm, the thicknesses for AlGaAsSb and InP were respectively 0.105 and 0.12 μm, giving a total mirror thickness of 5.52 μm. Since the stabilization of AlGaAsSb during the cooling phase of the reactor lead to a degradation of the surface morphology, the DBR was capped with InP of $\lambda/2$ thickness to avoid the Fabry–Pérot resonance in the stopband.

Table 1
Optimized growth conditions for the DBR growth

Parameters	InP	AlGaAsSb
Temperature	570 °C	
Reactor pressure	160 mbar	
Total flow	12 l/min	21.5 l/min
Gas velocity	1 m/s	1.75 m/s
V/III	217	0.5
Growth rate	1.24 μm/h	0.7 μm/h

3. Results

The absolute linear reflectivities measured with a photospectrometer (Varian Cary 5E), have been calibrated using three dielectric high reflectors, with stopbands covering the wavelength range from 1 to 1.58 μm. Measurements were performed along a radial line on three positions: (1) close to the center, (2) at 12–13 mm from the center and (3) at 2–3 mm from the wafer edge. This was repeated in the opposite direction, leading to a total of six measurements. To improve the accuracy of the measurements, the heights of the stopbands were calibrated at 1.535 μm using the nonlinear reflectivity measurement setup (NLR) [13]. In the NLR measurement a laser beam at 1.535 μm is focused on the DBR. A beam-splitter feeds a small part of the incident and reflected beam onto two photodiodes. The reflectivity is calculated from the ratio of the two photodiodes photocurrents. Since near the wafer edge the stopbands are shifted from 1.535 μm, measurements only at the center and at 12–13 mm from the center were performed. Signal integration and averaging improved the signal-to-noise value of the reflectivity measurement at this wavelength, giving a measurement error of

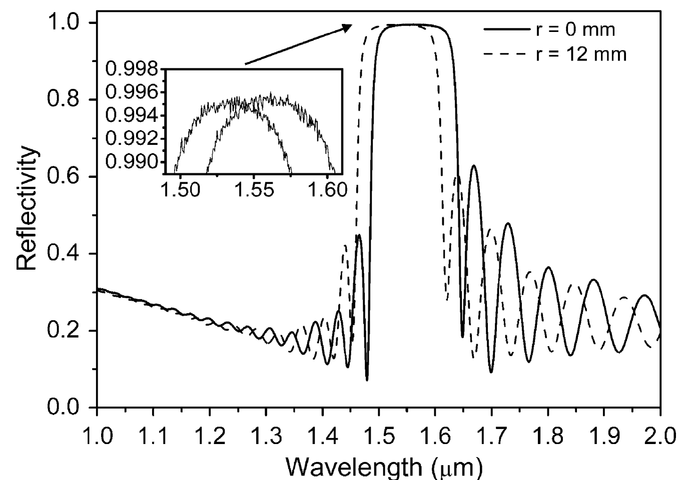

Fig. 4. Absolute linear reflectivity measurements of the DBR at the wafer center (solid line), and at 12 mm from center (dashed line).

0.03%. Fig. 4 illustrates the reflectivity measurements near the wafer center and at a displacement of 12–13 mm. In the center the maximum reflectivity (R_{max}) and the stopband width (SBW) are 99.54% and 157 nm, respectively. At 12–13 mm R_{max} was 99.51% and the SBW 153 nm. The measurements in the opposite direction showed a center R_{max} of 99.49% and 99.46% at 12–13 mm. The stopband at the edge of the wafer was blue-shifted by 90 nm, but still showed a reflectivity above 99%. This is not shown in Fig. 4 because precise calibration was possible only at 1.535 μm. The stopband height and the shape illustrated in the zoomed inset of Fig. 4 indicate that no absorption in the AlGaAsSb layers is present that could affect the reflectivity. Below 1.47 μm, the rapid damping of the oscillations' amplitude proves the absorption of the quaternary material. From these considerations we can conclude that the Al concentration did not decrease in growth direction, at least not by more than $\Delta x = 0.005-0.01$.

In order to quantify possible reflectivity losses due to residual absorptions, the transmission losses were measured by illuminating the DBR with a laser beam of 1 mm diameter at 1.535 μm and 300 mW. Since the backside of the wafer was unpolished, a fraction of the light was scattered. Therefore, an 8 mm high-numerical aperture (NA = 0.5) lens was introduced to collect the transmitted light. Moreover, it is taken into account that 30% of the light transmitted through the mirror is reflected at the InP–air interface. The measurements lead to 0.3–0.4% transmission losses. The nonlinear reflectivity (NLR) measured for incident pulse energy fluences from 0.3 to 30 $\mu J/cm^2$ proved that negligible (i.e. $<0.1\%$) residual valence-to-conduction-band absorption is present inside the DBRs stopband. Probably, the type-II band alignment between InP and AlGaAsSb also contributes to this residual absorption, since a broad type-II PL emission has been measured around 1.55 μm. With the average reflectivity of 99.5%, a transmission of 0.3–0.4%, and a saturable absorption lower than 0.1%, the remaining additional loss of 0–0.2%, have to be allocated to the insufficient accuracy of the transmission measurement, free-carrier absorption, or additional nonsaturable defect absorption in the DBR. Consequently, we expect that increasing the number of Bragg pairs can still increase the reflectivity.

Of high interest is the amount of traps and recombination centers at the interfaces and in the AlGaAsSb layers. Therefore time-resolved differential reflectivity measurements (pump-probe) in the absorbing region of AlGaAsSb at 1.35 and 1.4 μm have been performed with 280 fs pulses. We observed carrier lifetimes of several 100 ps, demonstrating the low defect concentration in the AlGaAsSb layers and the excellent interface quality.

Fig. 5 shows the HRXRD measurements of the DBR structure at three positions: in the center of the wafer at 12 mm and at 20 mm from the center. For all measurements, the highest peak centered at 0 arcsec corresponds to the diffraction of the InP layers and substrate. The sharpness of the fringe peaks indicates a good crystal and interface quality. Near the center, the peak of the AlGaAsSb layers is superimposed on that of the InP. This shows that the condition for lattice match is fulfilled and that no composition drift occurred in growth direction for the AlGaAsSb layers. However, the quaternary material becomes strained when we move from the center region to the edge of the wafer, shown by the AlGaAsSb-associated peak appearing to the right of the InP peak. Since the Al concentration has a negligible influence on the lattice constant, as mentioned in the introduction of Section 2, the shift of the peak in the HRXRD from center to the edge of the wafer is attributed to an increase of $\Delta y = 0.02$ of the As concentration. The averaged spacing between adjacent fringes revealed a thickness of 221 nm for the single-period AlGaAsSb/InP at the wafer center, whereas 208 nm is measured close to wafer edge. This result is coherent with the observed shift on the reflectivity stopband center discussed below. Because of the high number of parameters involved in the HRXRD simulation, the proper thickness variation of each quarter-wave layer could not be differentiated.

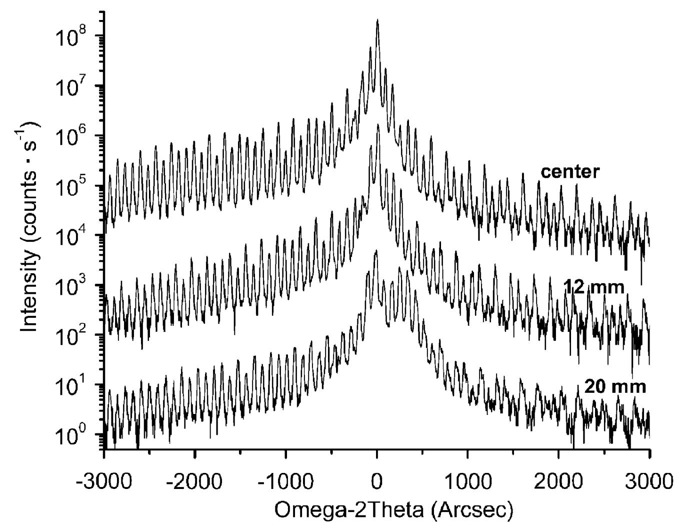

Fig. 5. HRXRD of the DBR at wafer center (top curve), at 12 mm (middle curve) and at 20 mm from the center (bottom curve).

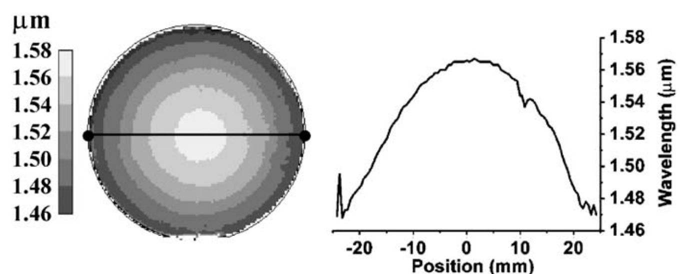

Fig. 6. Left: mapping of the SBC on 2 inch wafer. Right: SBC wavelength along the diagonal line drawn on the mapping.

Fig. 6 shows the mapping of the stopband center (SBC) wavelength. From the center to 20 mm from the center, the SBC shifts by approximately 80 nm to lower wavelength. By assuming a constant layer thickness and the observed increase of $\Delta y = 0.02$ in the As content, the SBC wavelength would decrease by only 1.6 nm (0.1% of 1.55 μm). Since no change of the Al concentration across the wafer is expected, the composition variations in the AlGaAsSb cannot account for the whole observed SBC wavelength shift of 80 nm. Therefore, we attribute this shift completely to an according thickness variation of the mirror layers of 5%.

The surface morphology observed under the optical microscope showed no crosshatch on the entire surface and practically no defects on more than 90% of the surface. The low lattice mismatch of AlGaAsSb caused by the As concentration increase of $\Delta y = 0.02$ and the expected grading of Sb in InP described above, were not sufficient to generate crosshatch.

4. Conclusions

In summary, different growth aspects of AlGaAsSb/InP as the Sb segregation-related effects, the stability and reproducibility for the composition, the decomposition of TMAl and Al incorporation, and the creation of defects have been studied. A growth process has been developed for stable conditions, which allowed to grow for the first time by MOVPE a highly reflective DBR at 1.55 μm composed of 24 AlGaAsSb/InP periods with an R_{max} of 99.54%. In AlGaAsSb, the As concentration increased by $\Delta y = 0.02$ from the center wafer to the edge, while the Al concentration was constant. The residual absorption due to free carrier absorption and nonsaturable defect absorption is between 0% and 0.2%, while the saturable absorption losses due to conduction-to-valence-band absorption are below 0.1%. The wafer surface appears free of any crosshatch and is over 90% defect-free. The performance of the DBR demonstrates the potential of high volume manufacture of more complex devices with these materials, including LW-VCSELs. Moreover, the achieved results for both $Al_{0-0.14}$GaAsSb and InP indicate that highly reflective DBRs at 1.3–1.5 μm and beyond, and other μm-thick heterostructures lattice-matched to InP, can be grown successfully by MOVPE.

Acknowledgments

The authors thank the Swiss National Center for Competence in Research (NCCR) for financing this project and Avalon Photonics Ltd for the collaboration.

References

[1] S. Nakagawa, E. Hall, G. Almuneau, J.K. Kim, D.A. Buell, H. Kroemer, L.A. Coldren, Appl. Phys. Lett. 78 (2001) 1337.
[2] M.W. Dvorak, C.R. Bolognesi, O.J. Pitts, S.P. Watkins, IEEE Electron. Dev. Lett. 22 (2001) 361.
[3] R. Grange, O. Ostinelli, M. Haiml, L. Krainer, G.J. Spühler, M. Ebnöther, E. Gini, S. Schön, U. Keller, Electron. Lett. 40 (2004) 1414.
[4] J.C. Zolper, J.F. Klem, T.A. Plut, C.P. Tigges, in: Proceedings of the IEEE First World Conference on Photovoltaic Energy Conversion, Waikoloa, HI, USA, 1994, p. 1843.
[5] B. Lambert, Y. Toudic, Y. Rouillard, M. Gauneau, M. Baudet, F. Alard, I. Valiente, J.C. Simon, Appl. Phys. Lett 66 (1995) 442.
[6] C. Agert, P. Lanyi, A.W. Bett, J. Crystal Growth 225 (2001) 426.
[7] R. Kaspi, K.R. Evans, J. Crystal Growth 175/176 (1997) 838.
[8] N. Watanabe, Y. Iwamura, Jpn. J. Appl. Phys. 35 (1996) 16.
[9] G.B. Stringfellow, M.J. Cherng, J. Crystal Growth 64 (1983) 413.
[10] M.J. Cherng, G.B. Stringfellow, R.M. Cohen, Appl. Phys. Lett. 44 (7) (1984) 677.
[11] D.W. Squire, C.S. Dulcey, M.C. Lin, J. Vac. Sci. Technol. B 3 (1985) 1513.
[12] F. Brunner, S. Weeke, M. Zorn, M. Weyers, J. Crystal Growth 272 (2004) 111.
[13] M. Haiml, R. Grange, U. Keller, Appl. Phys. B 79 (2004) 331.